# RESEARCH ARTICLE







15480569, 2022, 0, Downloaded from https://onlinelibrary.wiley.com. By University Of Tennessee, Knoxville- on [19/05/2022]. Re-use and distribution is strictly not permitted, except for Open Access articles and the stribution of the stribution of

# Anisotropic thermal behavior of extrusion-based large scale additively manufactured carbon-fiber reinforced thermoplastic structures

Ahmed Arabi Hassen<sup>1</sup> | Ralph B. Dinwiddie<sup>2</sup> | Seokpum Kim<sup>1</sup> | Halil Levent Tekinap<sup>1</sup> | Vipin Kumar<sup>1</sup> | John Lindahl<sup>1</sup> | Pritesh Yeole<sup>1,3</sup> | Chad Duty<sup>1,3</sup> | Uday Vaidya<sup>1,3</sup> | Hsin Wang<sup>2</sup> | Vlastimil Kunc<sup>1</sup>

#### Correspondence

Ahmed Arabi Hassen, Manufacturing Science Division, Oak Ridge National Laboratory, Oak Ridge, TN, USA. Email: hassenaa@ornl.gov

#### **Abstract**

Large format additive manufacturing (AM) enables rapid manufacturing of large parts and structures with minimum waste in material and energy. Extrusion-based AM deposition processes provide parts with highly anisotropic thermal properties, which are not typically reflected in textbook values for these materials. In order to develop accurate models that describe the directionally dependent thermal behavior of these materials in processing and service, accurate measurements of specific heat capacity and thermal conductivity are required. This work characterizes, documents, and analyzes the effect of the anisotropic nature of the extrusion-based deposition process on the specific heat capacity and thermal conductivity of the resulting AM products. All measurements were made over a temperature range of 20-180°C using the transient plane source technique, also referred to as the hot disk technique. Three of the most commonly used large format AM feedstock materials that utilize carbon fiber reinforcement were examined in this work: acrylonitrile butadiene styrene, polyphenylene sulfide and polyphenylsulfone. These findings can serve as a thermal design/process guideline for future large format AM applications.

# KEYWORDS

additive manufacturing, anisotropy, carbon fibers, short-fiber composites, thermal conductivity, thermal properties

Ahmed Arabi Hassen and Ralph B. Dinwiddie are the first authors with equal contributions.

Ralph B. Dinwiddie deceased on April, 2020.

This manuscript has been authored by UT-Battelle, LLC, under contract DE-AC05-00OR22725 with the US Department of Energy (DOE). The US government retains and the publisher, by accepting the article for publication, acknowledges that the US government retains a nonexclusive, paid-up, irrevocable, worldwide license to publish or reproduce the published form of this manuscript, or allow others to do so, for US government purposes. DOE will provide public access to these results of federally sponsored research in accordance with the DOE Public Access Plan (http://energy.gov/downloads/doe-public-access-plan).



<sup>&</sup>lt;sup>1</sup>Manufacturing Science Division, Oak Ridge National Laboratory, Oak Ridge, Tennessee, USA

<sup>&</sup>lt;sup>2</sup>Materials Science and Technology Division, Oak Ridge National Laboratory, Oak Ridge, Tennessee, USA

<sup>&</sup>lt;sup>3</sup>Department of Mechanical, Aerospace and Biomedical Engineering, University of Tennessee, Knoxville, Tennessee, USA

15480569, 2022, 0, Downloaded from https://onlinelibrary.wiley.com. By University Of Tennessee, Knoxville- on [19/05/2022]. Re-use and distribution is strictly not permitted, except for Open Access articles and the stribution of the stribution of

# 1 | INTRODUCTION

There is a growing interest in additive manufacturing (AM) and prototyping technologies for reducing product development cycle time, reducing production costs, and increasing manufacturing competitiveness. 1-5 Fused filament fabrication (FFF) is the most commonly used AM method as it utilizes less expensive machinery and costeffective thermoplastic feedstock materials. In FFF, semimolten thermoplastic filaments are extruded through a nozzle in a 2D plane and a 3D structure is achieved by successive layer-by-layer deposition of the material. Bonding between layers is caused by local re-melting of the previously solidified layer and diffusion of molecules across the interface. During deposition the extruded filament cools quickly, which affects adhesion and strength between layers.6 This repetitive heating and cooling cycle of multiple layers in the FFF process can induce significant residual stresses causing distortion or warpage of the part.7

FFF processes are limited by the rate at which the filament can be melted.8 This affects the deposition rate and, consequently reflects on the print size. Oak Ridge National Laboratory (ORNL) partnered with Cincinnati Incorporated to develop the big area additive manufacturing (BAAM) process that is based on extrusion deposition, see Figure 1A and Figure 1B. The system can print up to 16,000 cubic centimeters (1000 cubic inches) per hour and approximately 45.5 kg/h (100 pounds/h). To put this into perspective, conventional desktop sized FFF printers only have a deposition rate of 1-5 cubic inches per hour. The BAAM system enables rapid manufacturing of large parts (e.g., 6 m length  $\times$  2.5 m width  $\times$  1.8 m height). To achieve high deposition rates and large prints, pellet feedstock (<\$10/kg) is used. The feedstock material is typically a thermoplastic-based resin system reinforced with chopped carbon fiber. The carbon fiber increases the stiffness, strength,9 and thermal conductivity of the feedstock. 10,11 Carbon fiber (CF) reinforcement also provides dimensional stability<sup>12</sup> and reduces the coefficient of thermal expansion (CTE)<sup>13,14</sup> of the material. The deposition head for the BAAM system is a single screw polymer extruder with four heating zones, which is mounted on a large gantry system. Because of BAAM's large build volume and higher build rates, the system has been used in several application demonstrations such as Project Additive Manufacturing Integrated Energy (AMIE) (i.e., a project that involves the fabrication of a building and a utility vehicle).<sup>15</sup>

Recent developments in new material systems for AM and advances in AM systems have enabled tools (molds) and dies to become one of the most important and promising applications for AM technology. 9,16–18 Since the late 1990s, the U.S. tool and die industry has suffered from work shifting away overseas from the U.S. market. The BAAM technology shows promise as a commercially viable route to produce different types of tools and molds. 16–18 Tools and molds can be classified according to their service temperatures (e.g., room temperature, low temperature (<100°C), or high temperatures (>100°C)).

Carbon fiber reinforced acrylonitrile butadiene styrene (ABS) is the most common material used in the fabrication of BAAM components.<sup>3,19</sup> ABS is an amorphous polymer system with a relatively low glass transition temperature of 105°C, which makes it suitable for room temperature applications. However, a decrease in the dimensional stability of the fabricated part can be observed under elevated temperatures. Therefore, a number of high temperature polymers have been developed by ORNL and Techmer PM for large format AM applications, most notably CF reinforced polyphenylene sulfide (PPS) and polyphenylsulfone (PPSU).<sup>18</sup> These polymer systems provide enhanced dimensional stability under elevated temperatures and pressures (up to of 176.6°C (350°F) and, 620 kPa (90 psi))<sup>18</sup> that make them suitable materials for high temperature die and molds applications.

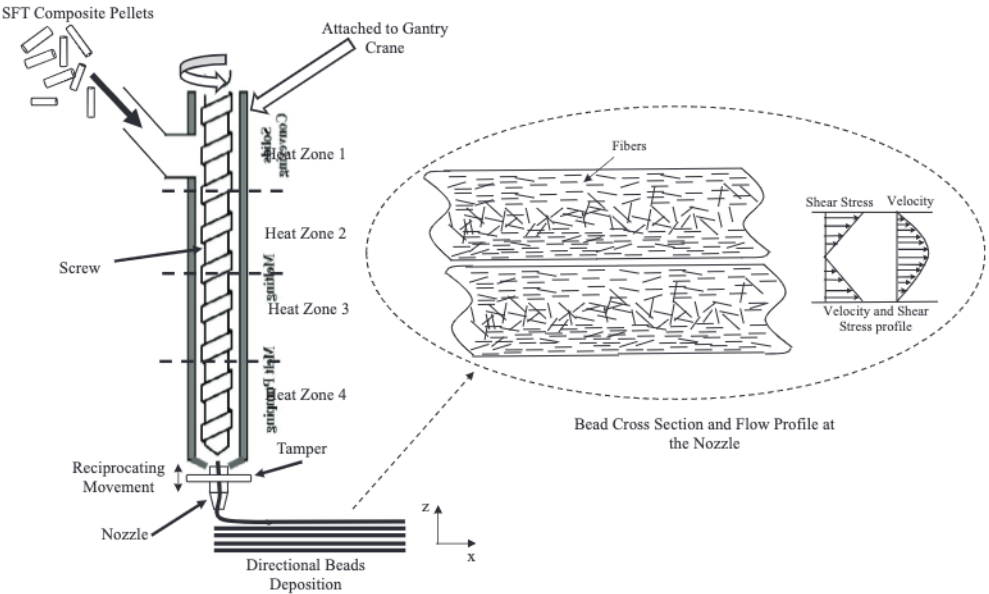
In AM extrusion depositions and FFF processes, the material is deposited in a directional manner, which





manufacturing (BAAM) system (build volume of: 3.6 m (length), 1.8 m (width), and 2.4 m (height)); (A) overview of the BAAM system, and (B) close view of the gantry system and the extruder setup

15480569, 2022, 0, Downloaded from https://onlinelibrary.wiley.com. By University Of Tennessee, Knoxville- on [19/05/2022]. Re-use and distribution is strictly not permitted, except for Open Access articles.



results in anisotropic properties, see Figure 2. The extruded material flows through a nozzle before the deposition process and the flow kinematics in the nozzle highly affect the fiber orientation in the final deposited bead.<sup>20,21</sup> Fibers have a tendency to strongly align with the flow direction near the nozzle wall but are less oriented at the center of the bead where shear forces are reduced (Figure 2). The mechanical and thermal properties of the resulting part depend strongly on the microstructure (i.e., fiber orientation) of the deposited composite. In mold and die applications, understanding the effect of the anisotropy on the thermal conductivity is crucial because it can result in non-uniform heating of the AM mold.

Thermal properties including thermal conductivity, specific heat capacity, and coefficient of thermal expansion (CTE) of CF reinforced composites are of great importance during their high temperature applications. Literature suggests that the thermal properties are also highly dependent on carbon fiber directions.<sup>22,23</sup> Pradere et al.24 explained that the CTE of CFs along the transverse direction varies from  $5 \times 10^{-6} \text{ K}^{-1} - 10 \times 10^{-6} \text{ K}^{-1}$ ; however, along the longitudinal direction offers lower expansion as  $1.6 \times 10^{-6}$ -  $2.1 \times 10^{-6}$  K<sup>-1</sup> based on the fiber properties. Bard et al.<sup>25</sup> showed that the thermal conductivity in transverse and fiber direction at different carbon volume fraction follow exponential and linear correlations, respectively. Researchers have also investigated the anisotropic thermal conductivity for 3D printed structures and reported that the print direction, filler volume fraction and filler morphology are some of the main factors responsible for the anisotropic behavior.<sup>26-28</sup> Shemelva et al. proposed to control the thermal conductivity through a combination of print raster direction and material design.<sup>29</sup> Most of the existing studies cover the effect of the anisotropic nature of the AM process on the thermal properties of small-scale FFF systems and the available literature provides very little information on large scale AM system (extrusion deposition based). This study aims to establish the basic understanding of the effect of the material anisotropy on the thermal conductivity of large-scale additively manufactured carbon fiber reinforced thermoplastic composites and demonstrate the variations in thermal conductivity in three main directions. These measurements take into account the carbon fiber alignment, which occurs during the deposition process, as well as porosity which may develop within or among the extruded beads. Such understanding will be extremely valuable in the design and process optimization. Moreover, the findings will assist in developing accurate predictive models that can describe the thermal behavior of these materials both during processing and/or in use of these materials in high temperature applications.

# MATERIALS AND SAMPLE **PREPARATION**

Samples used in this work were fabricated using the BAAM system. Three different discontinuous short fiber reinforced (i.e. average of 250 µm in length) thermoplastic materials were used in this work, namely ABS/CF 20% by weight (wt.), PPSU/CF 25% wt. and PPS/CF 50% wt. All thermoplastic pellets used in this study were compounded by Techmer PM. The materials are commercially available and are widely used for the BAAM system for molds and dies application. 9,17,18,30,31 The printing parameters were optimized based on previous trials to achieve uniform bead

TABLE 1 Temperature profile and printing parameters

	Material	Material		
Parameters	ABS/CF (20% wt.)	PPSU/CF (25% wt.)	PPS/CF (50% wt.)	
Screw speed (RPM)	250	250	250	
Bed temperature (°C)	100	100	100	
Printing speed (mm/s)	81	81	81	
Layer deposition time intervals (s)	120	120	120	
Total printing time (h)	2.5	2.5	2.5	
Nozzle diameter (mm)	10.16	10.16	10.16	
Bead size (mm)	12.7	12.7	12.7	
Temperature (°C)				
Zone 1	177	298	305	
Zone 2	177	332	321	
Zone 3	205	337	326	
Zone 4	232	343	337	
Zone (Tip)	249	354	337	
End use/application temperature	~85°-90°C	~121°-170°C	$\sim$ 121 $^{\circ}$ –170 $^{\circ}$ C	

extrusion and high dimensional stability and are listed in Table 1. In each case, a cube measuring 304.8 mm along each side was printed with a unidirectional orientation of the deposited beads (the deposition direction is defined as the X-direction). Smaller cubes with a side length of 50.8 mm were extracted from the blocks and all sides were machined (milled) flat.

# 3 | MATERIALS CHARACTERIZATION

All samples were tested at a temperature range from room temperature to the potential end use/application temperature for each AM composite feedstock, see Table 1. As an example, PPSU/CF 25% wt. and PPS/CF 50% wt. are used in additively manufactured autoclave tools that operate at 170°C (338 F) and 6.2 bar (90 psi) pressure.<sup>18</sup>

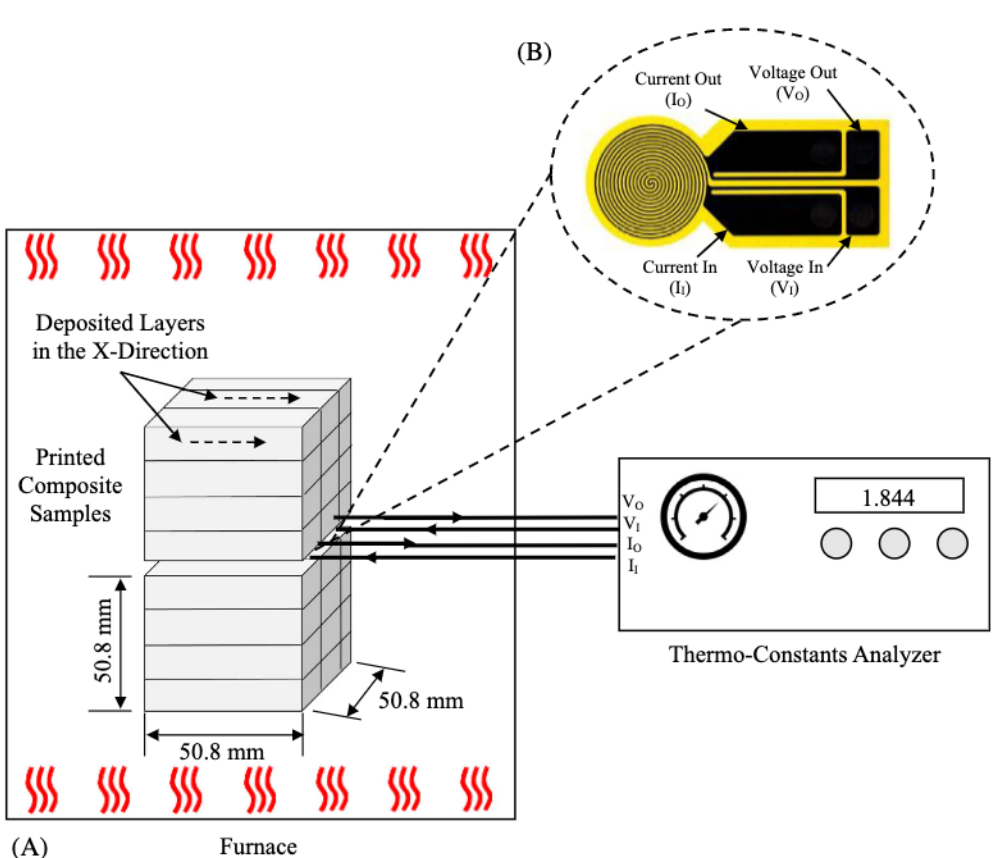
# 3.1 | Thermal conductivity

All thermophysical properties reported in this work were measured using a transient plane source (TPS) technique, Model TPS-3500. The TPS technique has been described with mathematical rigor elsewhere<sup>32</sup> and what follows is a brief overview containing the specific operational parameters used in this study. The TPS technique uses a thin film nickel bolometer sandwiched

within Kapton insulation, which serves as the sensor. In order to measure thermal conductivity and thermal diffusivity, this sensor is placed between two identical specimens and a modest load (4.4-6.7 N) is applied to the top specimen to assure adequate contact between the sensor and specimens, as shown in Figure 3. This sensor serves a dual role as a probe heater and a temperature sensor. During the measurement, the sensor coil is heated with a known amount of power and the coil's resistance is measured as a function of time. Using Equation 1, the temperature change,  $\Delta T(t)$ , resulting from this step heating can be calculated, since both the starting resistance  $(R_0)$  and the thermal coefficient of resistance  $(\alpha)$  are known, and the resistance as a function of time, R(t), is measured.

$$\Delta T(t) = \frac{1}{\infty} \left[ \frac{R(t)}{R_o} - 1 \right], \tag{1}$$

A typical temperature transient is shown in Figure 4. This transient consists of two regions: (1) an early response with a steep slope that is due to contact resistances from both the Kapton film and the sensor-specimen interface, and (2) a region in which the slope is slightly decreasing as a function of time. The temperature increase of the sensor is proportional to the power dissipated and inversely proportional to the thermal conductivity and diffusivity of the specimens. This second region is mathematically modeled using Equations 23 and 24 of Gustafsson's original paper on the technique.<sup>33</sup> Thus,



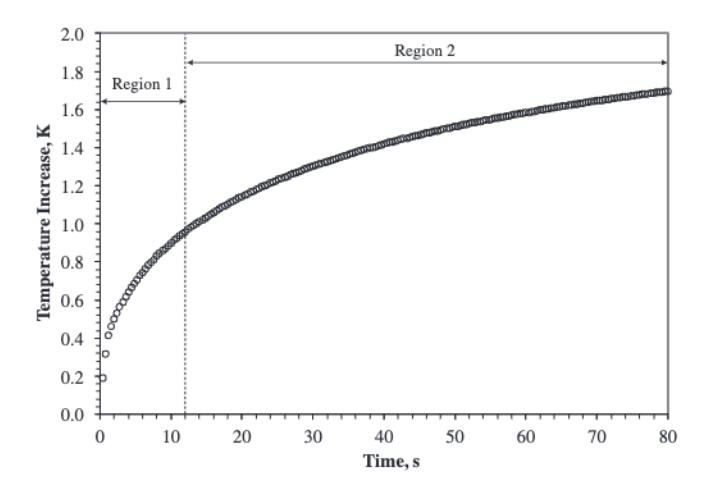


FIGURE 4 Typical temperature transient resulting from a step-heat pulse of a TPS sensor sandwiched between two room temperatures additively manufactured specimens of ABS/CF20%

thermal conductivity (K), thermal diffusivity (a) and volumetric heat capacity ( $rC_p$ ) of the specimens was calculated by curve fitting this model to the transient data in region II and the relationship:  $K = arC_p$ . In this study, the first 20–25 data points make up region I, as determined by observing the residuals from the curve-fitting algorithm.

The thermal conductivity of the composite specimens in this study was measured using a Kapton insulated sensor with a nickel heater/sensor with a 9.87 mm radius. (Hot Disk 8563). Typical scan times were selected as either 80s or 160 s, to optimize the probe depth of the measurement. Heating power was kept in the range of 70–90 mW. The measurements were taken 45 min apart, after the specimen stack was allowed for at least 12 h to equilibrate with the furnace. Specimen bulk temperatures were measured using a type-K thermocouple. For comparison, the standard TPS technique<sup>32</sup> was used to measure the room temperature thermal conductivity of neat ABS, PPSU, and PPS.

# 3.2 | Effect of AM anisotropy

The above discussion assumes the specimens are isotropic with lateral dimensions at least twice as large as the diameter of the sensor and a thickness greater than the sensor's radius. However, in the case of additively manufactured specimens, particularly with AM specimens containing fiber reinforcement, it is expected that the thermal conductivity will be different in three principle directions. As the materials being studied are not isotropic, an anisotropic analysis algorithm must be applied.<sup>33</sup> Assuming that a constant power supply is applied to a thin film, plane A from Figure 5, Equation 2 can be used to describe the behavior of the sensor under anisotropic conditions:

15480569, 2022, 0, Downloaded from https://onlinelibrary.wiley.com. By University Of Tennessee, Knoxville- on [19/05/2022]. Re-use and distribution is strictly not permitted, except for Open Access articles.

(A)

#### FIGURE 5

(A) Experimental setup for measuring the volumetric specific heat and (B) specific heat cell assembly. The volumetric specific heat is used to separate the axial thermal conductivity data from the radial contribution for the anisotropic thermal conductivity calculation

$$\frac{V}{V_{o}} = 1 + \frac{P_{o}\mu}{4h\sqrt{\pi}\sqrt{K_{1}K_{2}}}f(\tau_{2}), \qquad (2)$$

where  $V_0$  is the initial voltage across the sensor at time = 0, V is the measured voltage which increases due to the change in temperature and  $P_0$  is the constant power dissipated in the sensor of length h.  $\mu$  is the temperature depending resistivity of the thin film.  $K_1$  and  $K_2$ are the orthogonal thermal conductivities of the specimen in the plane of the sensor.  $\tau_2 = (t/Q_2)^{1/2}$ , where the characteristic time  $Q_2 = (d^2/a_2)$  where d is the radius of the sensor,  $a_2$  is the thermal diffusivity in the direction perpendicular to the plane of the sensor, and while  $K_3$  is the specimen thermal conductivity perpendicular to the plane of the sensor. Although  $K_3$  is not readily shown in Equation 2, it is a function of  $\tau_3$  and part of the  $f(\tau_3)$  term in Equation 3.  $\tau_3 = (t/Q_3)^{1/2}$ , where the characteristic time  $Q_3 = (d^2/a_3)$  where d is the radius of the sensor, and the thermal diffusivity in the direction perpendicular to the plane of the sensor  $a_3 = K_3/\rho C$ , where,  $\rho$  is the density and C is the volumetric heat capacity of the specimen.

$$\begin{split} f(\tau) &= \tau \operatorname{erf} \left(\tau^{-1}\right) - 0.5 \, \pi^{-\frac{1}{2}} \tau^2 \left[ 1 - \exp \left( -\tau^{-2} \right) \right] \\ &- 0.5 \, \pi^{-\frac{1}{2}} Ei \left( -\tau^{-2} \right). \end{split} \tag{3}$$

The integral functions are defined as,

$$\operatorname{erf}(u) = 2\pi^{-\frac{1}{2}} \int_{0}^{u} \exp(-v^{2}) dv, \tag{4}$$

$$-\mathrm{Ei}(-\mathbf{u}) = \int_{0}^{\infty} v^{-1} \exp(-v) dv. \tag{5}$$

Thus, by curve fitting T vs.  $f(\tau)$  (Equation 2), the product of the in-plane thermal conductivities  $(K_1 K_2)$  can be found from the slope and the through-plane thermal conductivity is found from  $f(\tau)$ .<sup>33</sup>

The calculation of radial (in-plane) thermal conductivity treats the thermal conductivity in the two orthogonal directions in the plane of the sensor  $(K_1 \text{ and } K_2)$ as indistinguishable. Since this is not the case in this study, the radial thermal conductivity calculation should be ignored. Whether or not this is valid mathematically and practically is the critical point of this work. In principle, the TPS method assumes finitely large specimen in all three directions. The calculation of perpendicular thermal conductivity  $K_3$  should not be affected by the in-plane thermal conductivity  $K_1$  and  $K_2$ no matter they are equal or not. In practice, the specimen dimensions are limited (a cube in this study). When  $K_1$  and  $K_2$  are not equal, the thermal wave will reach the boundaries at different times. It is important to manually control the probing depth to make sure the analysis range stay within the shorter heat propagation time in either directions. This was done by selecting limited number of points in region II of Figure 4 to ensure no boundary reflections affect the calculation. Therefore, the thermal conductivity in each principal direction of the specimen can be determined by making three separate measurements, where each of the principal axis being measured is aligned with the axial direction of the sensor.

In this work, the x-direction is defined as the direction parallel to the motion of the extruder (i.e., the axial direction). The z-direction is defined as the direction perpendicular to the plane of the extruded layers (interlayer direction, see Figure 2). Thus, the y-direction is perpendicular to both the extrusion direction (x) and the interlayer direction (z).

#### Volumetric specific heat 3.3

Volumetric specific heat was measured using a transient plane source sensor (Model: 5465) (sample diameter of 19-20 mm and thickness of 4-5 mm).33 The volumetric

15480569, 2022, 0, Downloaded from https://onlinelibrary.wiley.com. By University Of Tennessee, Knoxville- on [19/05/2022]. Re-use and distribution is strictly not permitted, except for Open Access articles.

specific heat is required for the anisotropic thermal conductivity calculation, as it is necessary to separate the axial thermal conductivity data from the radial contribution. The technique used to measure specific heat is described in detail elsewhere.<sup>33</sup>

A gold specific heat cell was used for this study, with approximate internal dimensions of a 21 mm diameter and 5 mm height (see Figure 5). First, the empty cell reference curve was obtained for a given temperature. A temperature increase in the range of 0.4-4°C is desired for accuracy. The power level used for the empty gold cell was 50 mW to raise the temperature by about 0.5°C in 40 s. The experiment was then repeated with the specimen-of-interest inside the gold cell. To obtain a similar temperature rise in 40 s once the specimen was added, the power level was increased to a range of 70-95 mW. During the scans, 200 data points were acquired for both the empty reference cell and the "cell + specimen." The linear portion of each scan (typically the last 100 data points) was used to determine the specific heat of the specimen. If the mass, volume and density of the specimen are known, the specific heat can be reported with units, J/K, J/kg K, and MJ/m<sup>3</sup> K. The physical dimensions, geometric volume, mass and density of each specimen is given in Table 2.

# 4 | RESULTS AND DISCUSSION

The measured specific heat values for neat ABS, PPSU and PPS at room temperature were 1333, 972, and 1028 J/kg K respectively. The temperature dependence of specific heat for all printed composite samples is listed in Table A1 and plotted in Figure 6, which shows that at room temperature, specific heat values for all neat polymers are higher than the AM composite sample values. This can be attributed to the integration of carbon fibers into these polymer systems. As an example, the value of specific heat for neat ABS is 1333 J/kg K and the specific heat of pan-based carbon fibers at room temperature has been reported as 726 J/kg K. Thus, a simple rule of mixtures based on weight fraction results in a predicted specific heat of 1215.4 J/kg K. This is within 1% of the measured value and well within the ±3% error of the

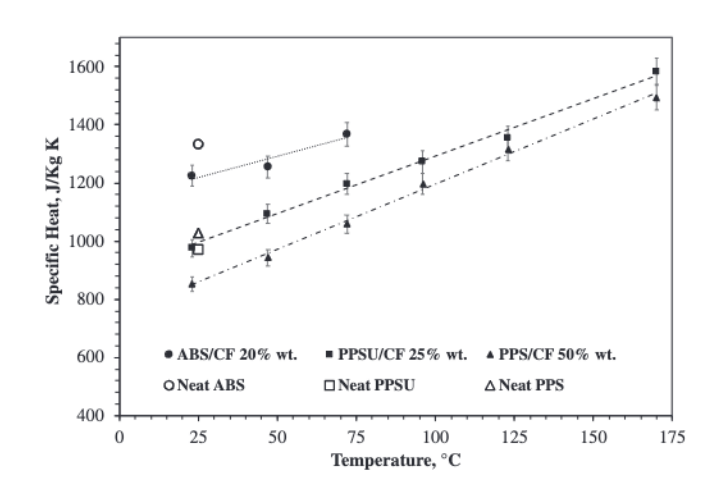


FIGURE 6 Specific heat of neat and additively manufactured ABS/CF 20% wt., PPSU/CF 25% wt. and PPS/CF 50% wt

experiment. Over the narrow temperature range of measurement, the specific heat of ABS/CF 20% wt. can be described by the empirical Equation (6) and shown in Figure 6.

$$C_{\rm v}({\rm ABS/CF}\,20\%{\rm wt.}) = 2.9293\,T + 1144.4\,({\rm J/kg}\,{\rm K}).$$
 (6)

Figure 6 shows the specific heat of the additively manufactured PPSU/CF 25% wt. samples as a function of temperature. The specific heat was found to increase linearly with temperature over the measured temperature range, as described by the empirical Equation 7 and shown in Figure 6.

$$C_{\rm v}(\text{PPSU/CF}25\%\text{wt.}) = 3.9579 \, T + 895.48 \, (\text{J/kgK}).$$
 (7)

The values of specific heat for the additively manufactured PPS/CF 50% wt. are also listed in Table A1 and shown in Figure 6. Once again, the specific heat increases linearly with temperature over the measured range, as described by Equation 8. For comparison, the specific heat of neat PPS is 1028 J/kg K, so the calculated mass weighted average for PPS/CF 50% wt. would be 886.5 J/kg K, which is within the experimental error of the measurement. Comparing all three thermoplastic composites showed that the composites with higher carbon fiber content resulted in larger reduction in specific heat compared to neat polymers.

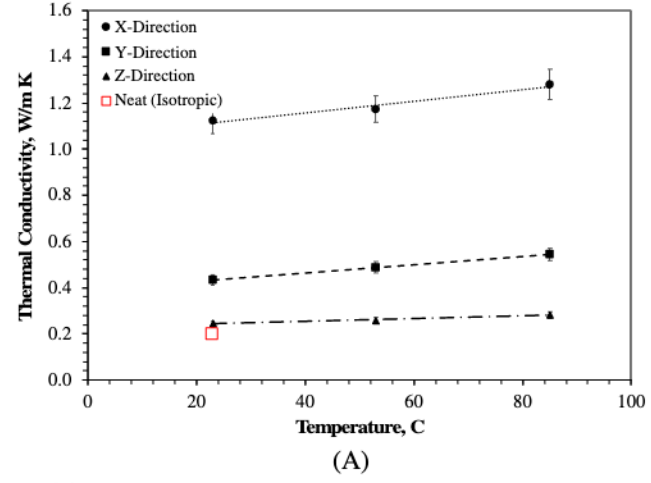
15480569, 2022, 0, Downloaded from https://onlinelibrary.wiley.com. By University Of Tennessee, Knoxville- on [19/05/2022]. Re-use and distribution is strictly not permitted, except for Open Access articles and the strict of t

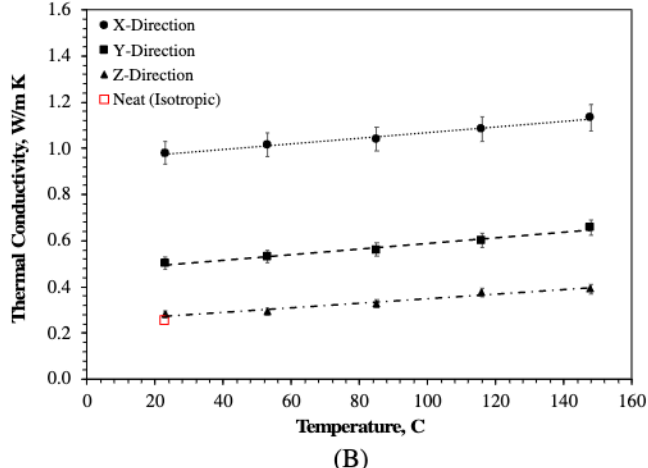
$$C_{\rm v}(PPS/CF50\%wt.) = 4.4942 T + 7.45.89 (J/kgK)$$
 (8)

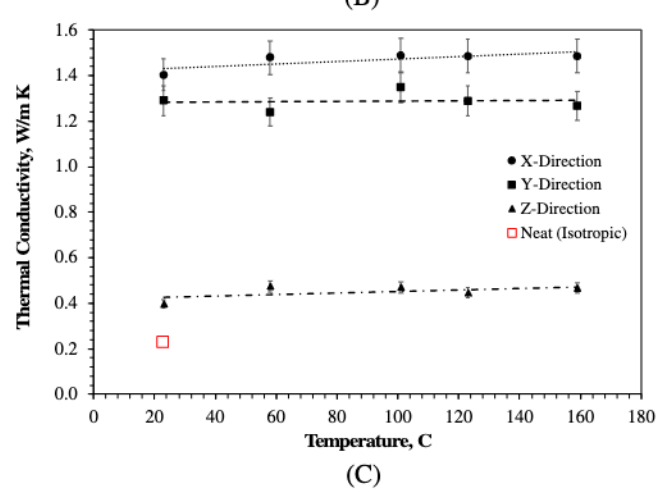
The thermal conductivity of additively manufactured samples was measured. The data can be compared to the measured values of neat polymer values listed in Table A2 and Figure 7. The temperature dependent anisotropic thermal conductivity values for all materials used in this work are given in Table A3 and Figure 7. It should be noticed that incorporating carbon fiber to the polymer enhanced the thermal conductivity of the composite when compared to the neat polymer. At all testing temperatures, the xdirection (extrusion direction) has the highest thermal conductivity while the z-direction (inter-layer direction) has the lowest value, as shown in Figure 7. Chopped fibers typically align in the extrusion direction and since carbon fibers have a significantly higher thermal conductivity than neat polymers, it is expected that the x-direction would have the highest thermal conductivity. Furthermore, during the extrusion and deposition process, the thickness of each newly extruded bead is reduced (approximately 50%) by a vertically vibrating a metal plate called the tamper (Figure 2). The goal of the tamper<sup>31</sup> is to increase the contact area between the previously deposited layer and the newly deposited layer.35

As indicated before, although only the perpendicular direction value was used in each measurement, the accuracy of anisotropic mode depends on the control of heat flow within the sample boundaries. For this study, the Y-Z planes thermal conductivities are much closer than the X direction. When the X-Y and X-Z surface are used to measure thermal conductivity in the Z and Y directions respectively, smaller number of points were used in calculation to satisfy the faster heat propagation in the Xdirection. This was done in practice by monitoring the residuals of the calculation to avoid the distinct boundary reflection curve. In valid calculation, the residuals were small in values and had random distributions. In the most recent revision of the ISO standard<sup>36</sup> of the TPS method, the modified anisotropic method used in this study has been developed into a forced one-dimensional (1D) measurement mode with a large circular or square sensor to cover the entire surface.

It has been reported that increasing the contact area increases the strength in the z-direction.<sup>37</sup> In this process, fibers have tendency for high preferential orientation at the direction of the deposition (x-direction). However, the use of the tamper partially squeezes the material out in the y-direction, and some fraction of the chopped fibers will preferentially align in the y-direction. Thus, it can be anticipated that the y-direction thermal conductivity is an intermediate value between the values for the xand z-directions. While we believe the fiber, orientation is the main factor for the variation in thermal conductivity in different directions, one should note that the

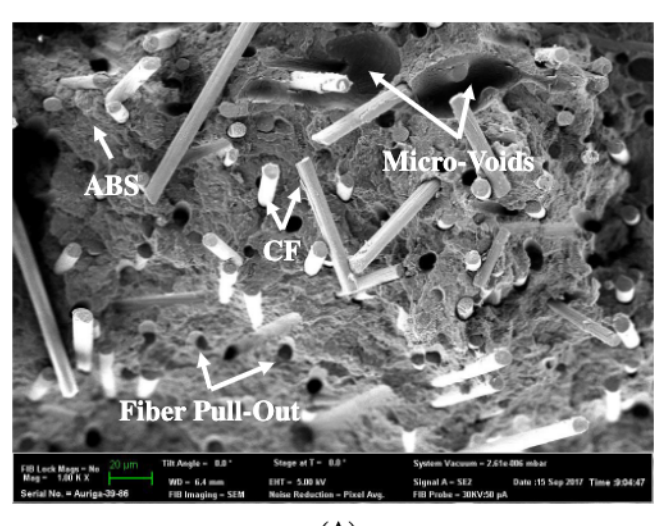




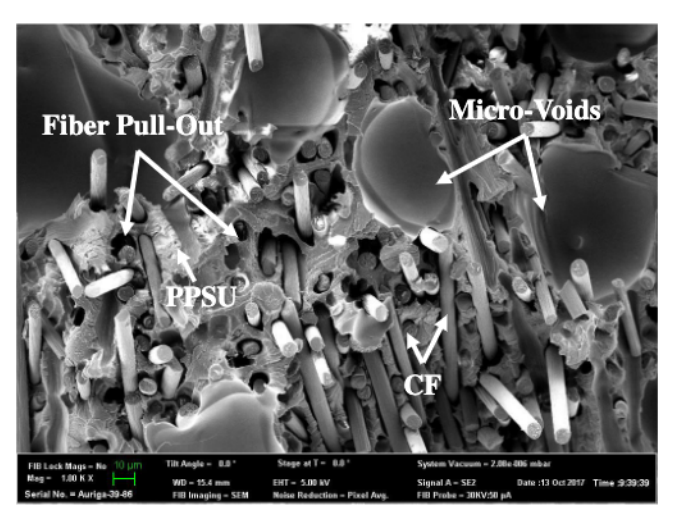


Anisotropic thermal conductivity of additively manufactured composites, (A) ABS/CF 20% wt., (B) PPSU/CF 25% wt. and (C) PPS/CF 50% wt

porosity, especially inter-bead porosity, and the bead-tobead thermal resistance also have a significant impact on the thermal conductivity of the composite. It is well known that porosity reduces the thermal conductivity,<sup>38</sup> and in AM extrusion deposition processes the porosity can be divided into two main categories.35 The first is microvoids, or inner-bead porosity, (i.e., entrapped air/gas



(A)



(B)

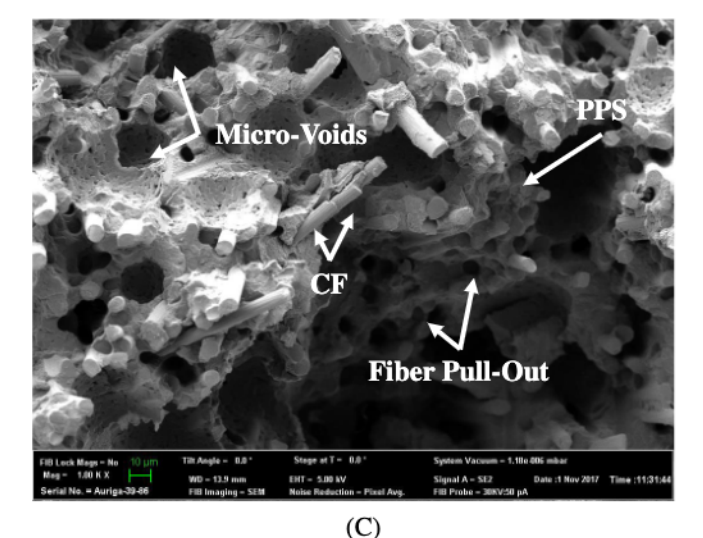


FIGURE 8 Scanning electron microscopy micrographs of fracture surfaces of printed beads, (A) ABS/CF 20% wt., (B) PPSU/ CF 25% wt. and (C) PPS/CF 50% wt. the graphs show micro voids induced in the samples during the additive manufacturing process

within the printed bead) that are introduced to the material during the compounding process or during the extrusion process (see Figure 8). The probability of the presence of void increases with the increase of the fiber content<sup>39</sup> and with the increase in the processing temperature.40 This can provide an explanation that while the three neat polymers have almost similar thermal conductivity, the ABS/CF 20% wt. has slightly higher thermal conductivity than PPSU/CF 25% wt. Moreover, this effect can be noticed for the thermal conductivity of PPS/CF 50% wt. when compared to the ABS/CF 20% wt. It can be noticed that the difference in thermal conductivity between the two campsites is just 25%, although, the PPS/CF 50% wt. has more than double the fiber content. This can be attributed to the increase of the porosity content that reflects on the thermal conductivity of the printed samples. The second type is macro-voids, or inter-bead porosity, diamond-shaped voids/channels along the xdirection, those form among the printed beads during the printing process (see Figure 9). Since the inter-bead pores are preferentially aligned in the x-y and x-z planes, they offer thermal resistance in the y- and z- directions. Similarly, since the beads are also aligned in the x-direction, bead-to-bead thermal resistance also inversely affecting the thermal conductivities in y- and z-directions.

The thermal conductivity in the x-, y- and z- directions can be fit in the form of the linear equations, Equation 9, Equation 10 and Equation 11, respectively (see Figure 7). As an example, the room temperature thermal conductivity of neat ABS is  $0.197 \pm 0.003$  W/m K and it increased by 470.6%, 120.3%, and 23.9% in x-, y- and z-direction, respectively for printed carbon fiber reinforced composite. Carbon fibers led to an increase in thermal conductivity in all three principle directions. The temperature dependence of the anisotropic thermal conductivity of additively manufactured ABS/CF 20% wt. is given in Table A3 and can be obtained in the three primary directions:

$$\lambda_x(ABS/CF20\%wt.) = 0.002525 T + 1.05681W/mK, (9)$$

$$\lambda_{v}(ABS/CF20\%wt.) = 0.001758 T + 0.39401W/mK (10)$$

$$\lambda_z(ABS/CF20\%wt.) = 0.0006144 T + 0.22836W/mK$$
(11)

The increase in the thermal conductivity of the material with the increase of temperature can be attributed to the increase in the value of specific heat (Figure 6) with increase in temperature. 41,42

The temperature dependence of the anisotropic thermal conductivity of additively manufactured PPSU/CF 25% wt. is given in Table A3 and shown in Figure 7B. WILEY—SPE INSPIRING PRASTIC.

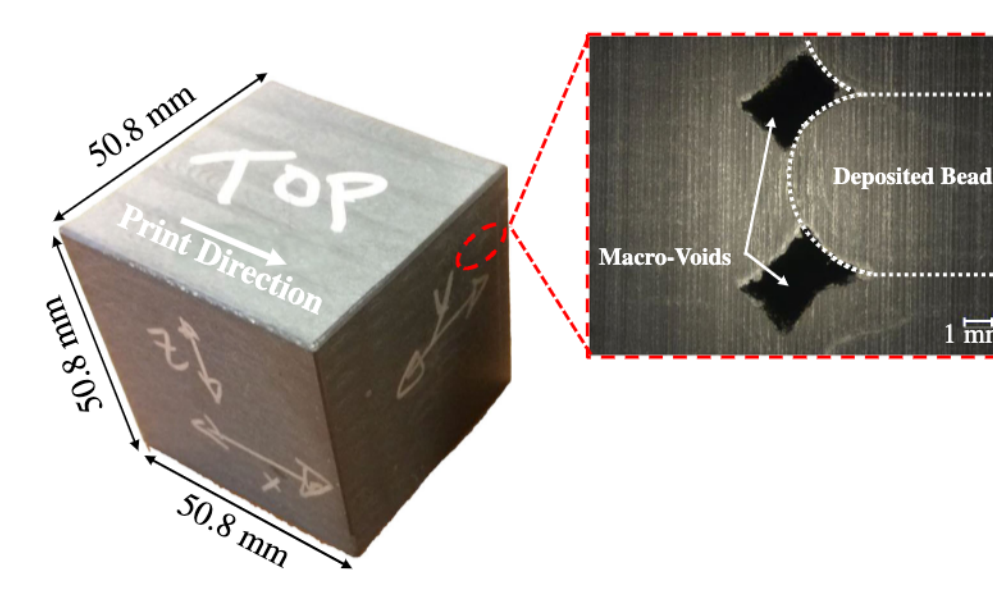


FIGURE 9 Image of an additively manufactured cube used for the thermal conductivity measurements; a micrograph shows a diamondshaped void formation at the print direction. The diamondshaped void contributes to the thermal conductivity values reported in this work

Similar to ABS/CF 20% wt., the x-direction value exhibits the highest thermal conductivity with 247.5% increase in thermal conductivity when compared to the z-direction values at room temperature. The thermal conductivity in each direction increases slightly with temperature and can be described using linear equations Equations 12-14). The room temperature thermal conductivity for neat PPSU is 0.255 ± 0.001 W/m K and an increase of 248.3% at the thermal conductivity was observed for the x-direction at room temperature 25% by wt. carbon fiber was added to the polymer.

$$\lambda_x(PPSU/CF25\%wt.) = 0.001200 T + 0.9484W/mK$$
 (12)

$$\lambda_{\nu}(PPSU/CF25\%wt.) = 0.001209 T + 0.4679W/mK$$
 (13)

$$\lambda_z(PPSU/CF25\%wt.) = 0.0009559 T + 0.2527W/mK$$
 (14)

The anisotropic thermal conductivity of additively manufactured PPS/CF 50% wt. is shown in Figure 7C. As with the other specimens, the x-direction is the highest and the z-direction is the lowest. The thermal conductivity is nearly constant with temperature (i.e., only an increase of 5% at the x-direction was noticed when heated from room temperature to 159°C). The linear curve fits are given in Equation 15-17. It should be noted that the 50% wt. carbon fiber has greatly increased the thermal conductivity in all directions from the room temperature value of neat PPS, which is  $0.228 \pm 0.002$  W/m K.

$$\lambda_x(PPS/CF50\%wt.) = 5.2945E - 04 T + 1.4190W/mK$$
 (15)

$$\lambda_y(PPS/CF 50\%wt.) = 6.9904E - 05 T + 1.2803W/mK$$

(16)

$$\lambda_z(PPS/CF 50\%wt.) = 3.3712E - 04 T + 0.41906W/mK$$
(17)

1 mm

### CONCLUSIONS

This study investigated the anisotropic nature of the extrusion-based deposition process on the thermal properties of printed structures. A novel technique using the volumetric specific heat was used to separate the axial thermal conductivity data from the radial contribution for in order to calculate the anisotropic thermal conductivity. The results showed that the specific heat of the three carbon fibers reinforced thermoplastics increased linearly with temperature and the thermal conductivity in the xdirection was significantly higher than the other two principal directions. The presence and relative alignment of carbon fibers within the printed part was considered primarily responsible for the thermal anisotropy. The addition of carbon fibers increases the thermal conductivity of each material by a factor of  $3\times$  to  $7\times$ , depending upon the orientation. Due to the alignment of carbon fibers in the x-direction, the thermal conductivity was found to be  $3\times$  to  $4\times$  higher than the other directions. The presented research provides constitutive equations to describe the specific heat and conductivity of each material with respect to temperature in each of the primary directions. This type of input is critical for the development of predictive models of thermal gradients during the printing process and in-service applications, which can be utilized in design and process optimization.

#### ACKNOWLEDGMENTS

This research was supported by the DOE Office of Energy Efficiency and Renewable Energy (EERE), Advanced Manufacturing Office under contract DE-AC05-00OR22725 with UT-Battelle LLC and used resources at the Manufacturing Demonstration Facility, a DOE-EERE User Facility at Oak Ridge National Laboratory. For large format additive manufacturing, the printing equipment was provided by Cincinnati Incorporated, a manufacturer of metal and additive manufacturing equipment, headquartered in Harrison, Ohio (https://www.e-ci.com). The printing material was provided by Techmer PM, a material design and manufacture company headquartered in Clinton, TN.

# ORCID

Ahmed Arabi Hassen https://orcid.org/0000-0003-2852-1222

#### REFERENCES

- W. Zhang, A. S. Wu, J. Sun, Z. Quan, B. Gu, B. Sun, C. Cotton,
   D. Heider, T. W. Chou, Compos. Sci. Technol. 2017, 150, 102.
- [2] F. Ning, W. Cong, J. Qiu, J. Wei, S. Wang, Compos. Part B 2015, 80, 369.
- [3] H. Tekinalp et al., Compos. Sci. Technol. 2014, 105, 144.
- [4] Z. Quan, Z. Larimore, A. Wu, J. Yu, X. Qin, M. Mirotznik, J. Suhr, J. H. Byun, Y. Oh, T. W. Chou, Compos. Sci. Technol. 2016, 126, 139.
- [5] L. Li, A. Tirado, I. C. Nlebedim, O. Rios, B. Post, V. Kunc, R. R. Lowden, E. Lara-Curzio, R. Fredette, J. Ormerod, T. A. Lograsso, M. P. Paranthaman, Sci. Rep. 2016, 6, 36212.
- [6] M. D. Monzón, I. Gibson, A. N. Benítez, L. Lorenzo, P. M. Hernández, M. D. Marrero, Int. J. Adv. Manuf. Technol. 2013, 67, 2717.
- [7] Y. Zhang, K. Chou, Proc. Inst. Mech. Eng. B J. Eng. Manuf. 2008, 222, 959.
- [8] J. Go, S. N. Schiffres, A. G. Stevens, A. J. Hart, Addit. Manuf. 2017, 16, 1.
- [9] Hassen, A.A., Lindahl J, Chen X, Post B, Love L, Kunc V, SAMPE Conf, Long Beach, CA 2016.
- [10] S. Han, D. D. L. Chung, Compos. Sci. Technol. 2011, 71, 1944.
- [11] S. Hind, F. Robitaille, Polym. Compos. 2010, 31, 847.
- [12] L. Love, C. E. Duty, B. K. Post, R. F. Lind, P. D. Lloyd, V. Kunc, W. H. Peter, C. A. Blue, Breaking barriers in polymer additive manufacturing, Oak Ridge National Laboratory (ORNL), Oak Ridge 2015.
- [13] D. J. Miller, Compos. Tool. 2015.
- [14] G. Velez-Garcia, A. Wright, V. Kunc, C. Duty, Coefficient of thermal expansion test report, ORNL, Oak Ridge, TN 2014.
- [15] K. Biswas, J. Rose, L. Eikevik, M. Guerguis, P. Enquist, B. Lee, L. Love, J. Green, R. Jackson, J. Sol. Energy Eng. 2017, 139(1), 15001.
- [16] V. Kunc, A. A. Hassen, J. Lindahl, S. Kim, B. Post, L. Love, 15th Japan International SAMPE Symposium and Exhibition, SAMPE, Japan 2017.
- [17] A. A. Hassen, R. Springfield, J. Lindahl, B. Post, L. Love, C. Duty, U. Vaidya, R. B. Pipes, V. Kunc, *CAMX Conference*, SAMPE, Anaheim, CA 2016.
- [18] V. Kunc, J. Lindahl, R. Dinwiddie, B. Post, L. Love, M. Matlack, R. L. Fahey, A. A. Hassen, CAMX Conference, SAMPE, Anaheim, CA 2016.

- [19] V. Kishore, C. Ajinjeru, A. Nycz, B. Post, J. Lindahl, V. Kunc, C. Duty, Addit. Manuf. 2017, 14, 7.
- [20] H. SadAbadi, M. Ghasemi, J. Reinf. Plast. Compos. 2007, 26, 1729.
- [21] A. N. Oumer, O. Mamat, Asian J. Sci. Res. 2013, 6, 401.
- [22] A. Tezvergil, L. V. Lassila, P. K. J. D. M. Vallittu, Dent. Mater. 2003, 19, 471.
- [23] R. Joven, SAMPE International Symposium Proceedings, SAMPE, Charleston, SC 2011.
- [24] C. Pradere, C. Sauder, Carbon 2008, 46, 1874.
- [25] F. S. Bard Simon, Mater. Des. 2019, 12, 1084.
- [26] M. R. Ahmed Elkholy, R. Kempers, Prog. Addit. Manuf. 2019, 4, 497.
- [27] M. Smith, S. Kim, A. Lambert, M. Walde, J. Lindahl, K. Mungale, T. Bougher, A. A. Hassen, V. Kunc, 8th IEEE Intersociety Conference on Thermal and Thermomechanical Phenomena in Electronic Systems (ITherm), IEEE, NV, USA 2019.
- [28] D. R. Hardikkumar Prajapati, R. L. Woods, A. Jain, Addit. Manuf. 2018, 21, 84.
- [29] C. Shemelya, A. De La Rosa, A. R. Torrado, K. Yu, J. Domanowski, P. J. Bonacuse, R. E. Martin, M. Juhasz, F. Hurwitz, R. B. Wicker, B. Conner, Addit. Manuf. 2017, 16, 186.
- [30] C. Ajinjeru, V.K., P. Liu, J. Lindahl, A. Hassen, Addit. Manuf., 2018, 21, 125.
- [31] C. Duty et al., Rapid Prototyp. J. 2017, 23(1), 181.
- [32] S. E. Gustafsson, Rev. Sci. Instrum. 1991, 62, 797.
- [33] S. E. Gustafsson, E. Karawacki, M. N. Khan, J. Appl. Phys. 1981, 52, 2596.
- [34] C. Pradère, J. M. Goyhénèche, J. C. Batsale, S. Dilhaire, R. Pailler, Rev. Sci. Instrum. 2005, 76, 064901.
- [35] A. A. Hassen, M. M. Kirka, Mater. Eval. 2018, 76, 438.
- [36] ISO/WD, Plastics—Determination of thermal conductivity and thermal diffusivity—Part 7: Determination of thermal effusivity by transient plane heat source (hot disc) method, in ISO/WD 22007-7, ISO, 2021 under devlopment.
- [37] C. E. Duty, V. Kunc, B. Compton, B. Post, D. Erdman, R. Smith, R. Lind, P. Lloyd, L. Love, *Rapid Prototyp. J.* 2017, 23(1), 181.
- [38] K. W. Schlichting, N. P. Padture, P. G. Klemens, J. Mater. Sci. 2001, 36, 3003.
- [39] A. Vaxman, M. Narkis, A. Siegmann, S. Kenig, *Polym. Compos.* 1989, 10, 449.
- [40] S. Roychowdhury, J. W. Gillespie, S. G. Advani, Computer Aided Design in Composite Material Technology III, Springer, Dordrecht 1992, p. 89.
- [41] R. Agarwal, N. S. Saxena, K. B. Sharma, S. Thomas, M. S. Sreekala, J. Appl. Polym. Sci. 2003, 89, 1708.
- [42] W. N. dos Santos, J. A. De Sousa, R. Gregorio Jr., Polym. Test. 2013, 32, 987.

How to cite this article: A. A. Hassen, R. B. Dinwiddie, S. Kim, H. L. Tekinap, V. Kumar, J. Lindahl, P. Yeole, C. Duty, U. Vaidya, H. Wang, V. Kunc, *Polym. Compos.* 2022, 1. <a href="https://doi.org/10.1002/pc.26645">https://doi.org/10.1002/pc.26645</a>



15480569, 2022, 0, Downloaded from https://onlinelibrary.wiley.com. By University Of Tennessee, Knoxville- on [19/05/2022]. Re-use and distribution is strictly not permitted, except for Open Access articl

# APPENDIX A

TABLE A1 Specific heat data for ABS/CF 20% wt., PPSU/CF 25% wt. and PPS/CF 50% wt.

ABS/CF 20% wt.					
Temperature (°C)	Specific heat capacity (J/K)	Specific heat per unit mass (J/kg K)	Volumetric specific heat (MJ/m³ K)	∆temp. Reference cell (K)	∆temp. Cell + sample (K)
23	$1.69 \pm 0.004$	1225 ± 2.7	$1.32 \pm 0.003$	0.57	0.47
47	$1.73 \pm 0.003$	$1256 \pm 2.4$	$1.41 \pm 0.003$	0.55	0.57
72	$1.89\pm0.003$	$1368 \pm 2.2$	$1.47 \pm 0.002$	0.59	0.68
PPSU/CF 25% wt.					
23	$1.45\pm0.001$	$976 \pm 0.1$	$1.05 \pm 0.001$	0.58	0.50
47	$1.62 \pm 0.015$	$1094 \pm 10.1$	$1.13 \pm 0.001$	0.55	0.53
72	$1.77\pm0.002$	$1196 \pm 1.4$	$1.28 \pm 0.002$	0.53	0.49
96	$1.89\pm0.006$	$1273 \pm 4.1$	$1.37 \pm 0.004$	0.51	0.47
123	$2.01\pm0.004$	$1354 \pm 2.8$	$1.45 \pm 0.003$	0.49	0.47
169	$2.35 \pm 0.001$	$1582 \pm 1.0$	$1.69 \pm 0.001$	0.46	0.47
PPS/CF 50% wt.					
23	$1.32\pm0.002$	$853 \pm 1.2$	$0.97 \pm 0.002$	0.58	0.58
47	$1.47 \pm 0.003$	944 ± 2.2	$1.07 \pm 0.002$	0.55	0.54
72	$1.64 \pm 0.002$	$1058 \pm 1.4$	$1.20 \pm 0.002$	0.53	0.51
96	$1.86 \pm 0.002$	$1197 \pm 1.0$	$1.36 \pm 0.002$	0.51	0.47
123	$2.04 \pm 0.001$	$1315 \pm 0.1$	$1.49 \pm 0.001$	0.49	0.45
170	$2.33 \pm 0.004$	$1495 \pm 2.8$	$1.69 \pm 0.003$	0.46	0.47

TABLE A2 Thermal conductivity of neat polymer

Polymer	Temperature (°C)	Thermal conductivity (W/m K)
ABS	23	$0.19 \pm 0.003$
PPSU	23	$0.26 \pm 0.001$
PPS	23	$0.23 \pm 0.002$





**TABLE A3** Temperature dependence of the anisotropic thermal conductivity of ABS/CF 20% wt., PPSU/CF 25% wt. and PPS/CF 50% wt.

ABS/CF 20% wt.				
Temperature (°C)	X-direction (W/m K)	Y-direction (W/m K)	Z-direction (W/m K)	
23	$1.12 \pm 0.021$	$0.43 \pm 0.005$	$0.24 \pm 0.001$	
53	$1.17 \pm 0.003$	$0.49 \pm 0.003$	$0.26 \pm 0.001$	
85	$1.28 \pm 0.060$	$0.54 \pm 0.007$	$0.28 \pm 0.004$	
PPSU/CF 25% wt.				
23	$0.98 \pm 0.008$	$0.50 \pm 0.007$	$0.28 \pm 0.007$	
53	$1.02 \pm 0.011$	$0.53 \pm 0.006$	$0.29 \pm 0.003$	
85	$1.04 \pm 0.016$	$0.56 \pm 0.004$	$0.33 \pm 0.012$	
116	$1.05 \pm 0.028$	$0.60 \pm 0.011$	$0.38 \pm 0.011$	
148	$1.13 \pm 0.033$	$0.66 \pm 0.009$	$0.39 \pm 0.015$	
PPS/CF 50% wt.				
23	$1.40 \pm 0.040$	$1.29 \pm 0.017$	$0.39 \pm 0.005$	
58	$1.48 \pm 0.017$	$1.24 \pm 0.022$	$0.47 \pm 0.004$	
99	$1.49 \pm 0.026$	$1.35 \pm 0.009$	$0.46 \pm 0.009$	
123	$1.49 \pm 0.040$	$1.29 \pm 0.061$	$0.45 \pm 0.004$	
159	$1.49 \pm 0.007$	$1.27 \pm 0.010$	$0.47 \pm 0.006$	

